X-Ray Evidence Against the Hypothesis that the Hyperluminous $z = 6.3$ Quasar J0100+2802 is Lensed

Thomas Connor[1,4] , Daniel Stern[1] , Eduardo Bañados[2] , and Chiara Mazzucchelli[3]

[1] Jet Propulsion Laboratory, California Institute of Technology, 4800 Oak Grove Drive, Pasadena, CA 91109, USA; thomas.p.connor@jpl.nasa.gov
[2] Max Planck Institute for Astronomy, Königstuhl 17, D-69117 Heidelberg, Germany
[3] European Southern Observatory, Alonso de Cordova 3107, Vitacura, Region Metropolitana, Chile

Abstract

The $z = 6.327$ quasar SDSS J010013.02+280225.8 (hereafter J0100+2802) is believed to be powered by a black hole more massive than $10^{10} M_\odot$, making it the most massive black hole known in the first billion years of the universe. However, recent high-resolution ALMA imaging shows four structures at the location of this quasar, potentially implying that it is lensed with a magnification of $\mu \sim 450$ and thus its black hole is significantly less massive. Furthermore, for the underlying distribution of magnifications of $z \gtrsim 6$ quasars to produce such an extreme value, theoretical models predict that a larger number of quasars in this epoch should be lensed, implying further overestimates of early black hole masses. To provide an independent constraint on the possibility that J0100+2802 is lensed, we reanalyzed archival XMM-Newton observations of the quasar and compared the expected ratios of X-ray luminosity to rest-frame UV and IR luminosities. For both cases, J0100+2802's X-ray flux is consistent with the no-lensing scenario; while this could be explained by J0100+2802 being X-ray faint, we find it does not have the X-ray or optical spectral features expected for an X-ray faint quasar. Finally, we compare the overall distribution of X-ray fluxes for known, typical $z \gtrsim 6$ quasars. We find a 3σ tension between the observed and predicted X-ray-to-UV flux ratios when adopting the magnification probability distribution required to produce a $\mu = 450$ quasar.

Unified Astronomy Thesaurus concepts: Quasars (1319); Strong gravitational lensing (1643); X-ray quasars (1821); Scaling relations (2031); X-ray astronomy (1810)

1. Introduction

The growing census of quasars known in the first billion years of the universe ($z \gtrsim 6$) has led to significant insights into the early universe, from how supermassive black holes (SMBHs) grow and evolve to the role that active galactic nuclei (AGN) play in processing the environments around the first massive galaxies. To date, over 200 quasars are known at $z > 6$ (e.g., Bañados et al. 2016); the most distant of these, at $z = 7.64$, has mass $M_{BH} = 1.6 \times 10^9 M_\odot$, comparable to the most massive black holes in the local universe (Wang et al. 2021a). These results are challenging to black hole formation models as, assuming Eddington-limited growth, a seed black hole formed 100 Myr after the Big Bang would require an initial mass greater than $10^4 M_\odot$ to produce the $z = 7.64$ quasar.

Chief among the high-redshift quasars is SDSS J010013.02+280225.8 (hereafter J0100+2802), a hyperluminous ($L_{bol} > 10^{48}$ erg s^{-1}), $z \sim 6.3$ quasar with a Mg II-derived mass of $M_{BH} \sim 1.2 \times 10^{10} M_\odot$ (Wu et al. 2015). As shown in Figure 1, it is, by far, the most massive black hole known at $z \gtrsim 6$. While, assuming Eddington-limited growth, J0100+2802 does not set the most stringent limits on the seeds of early black holes, its significant mass does, nevertheless, require rapid growth to have been occurring from seed formation to 850 Myr after the Big Bang. Based on imaging with the Atacama Large Millimeter/ submillimeter Array (ALMA), Wang et al. (2019) measured a

kinematic mass for J0100+2802's host galaxy of $M_{dyn} \sim 3.3 \times 10^{10} M_\odot$. This value is comparable to other high-z quasar host galaxies, although the implied black hole to dynamical mass fraction of $\sim 35\%$ is the largest value observed at $z \gtrsim 6$ (e.g., Willott et al. 2015).

Recently, Fujimoto et al. (2020) reanalyzed the ALMA observations of J0100+2802. In contrast to Wang et al. (2019), Fujimoto et al. (2020) generated higher-resolution images by utilizing Briggs weighting with a robust parameter of 0.2, resulting in a synthesized beam size of $0\rlap{.}''21 \times 0\rlap{.}''09$. In the new, higher-resolution maps, Fujimoto et al. (2020) resolved J0100+2802 into a compact quadruple system within a radius of $\sim 0\rlap{.}''2$. They proposed two explanations for this: either there are multiple, dusty star-forming regions in J0100+2802's host galaxy or the quasar has been lensed into a quad. They argued for the latter on account of emission and absorption features from a foreground $z = 2.33$ object in the quasar's spectrum. The mass model from HST imaging implies a magnification of $\mu \sim 450$. Such a magnification is extreme, with the closest analog coming from Glikman et al. (2018), who report a $z = 2.5$ quad-lensed quasar that is magnified by a factor of $\mu \sim 100$. This value also dwarfs that of UHS J0439+1634, the only reionization-era quasar known to be lensed, which has a magnification of $\mu \sim 50$ (Fan et al. 2019).

If J0100+2802 is lensed, a magnification of $\mu \sim 450$ would be significant; as the black hole mass estimate is based partially on the quasar's luminosity, this would imply $M_{BH} < 10^9 M_\odot$. And not only does $\mu \sim 450$ for J0100+2802 remove one of the strongest pieces of evidence for significant mass growth in late-stage reionization, but it could also imply broader trends; Pacucci & Loeb (2020) argue that, for a $\mu \sim 450$ quasar to exist, the expected distribution of magnification values would
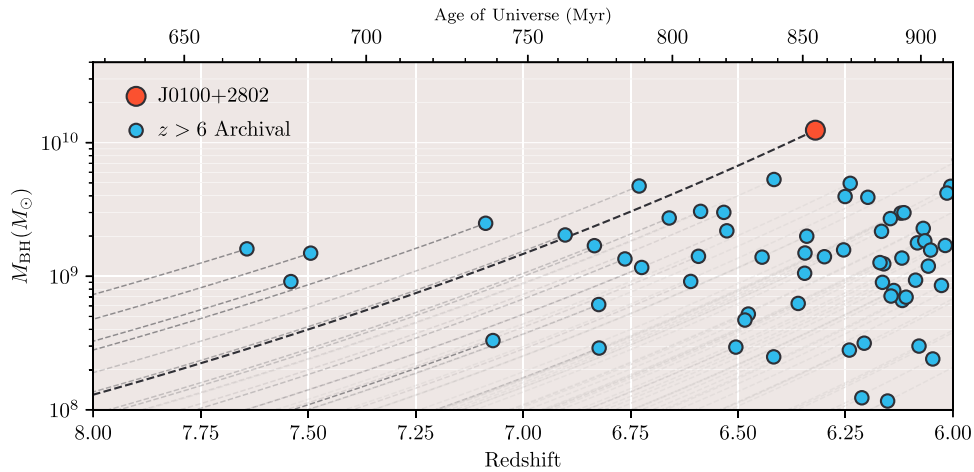
---

[4] NPP Fellow.

Figure 1. Mass and redshift of J0100+2802 (red), in comparison to a near-complete sample of $z > 6$ quasars currently known with robust, Mg II-derived black hole mass estimates (blue). For all quasars, a mass growth track is shown with dashed lines, depicting the expected mass of the black hole at earlier times, assuming constant Eddington-limited growth with an efficiency of 0.1. While J0100+2802 does not set the most stringent constraints on seed masses, it does nevertheless require significant, sustained growth through the entire epoch of reionization.

require that more of the $z > 6$ quasar population is lensed by $\mu \gtrsim 10$.

So far, the strongest rebuttal to the proposed lensing explanation for J0100+2802 comes from Davies et al. (2020). They point to the proximity zone of the quasar, the region around the AGN that has been substantially overionized, leading to a deficit in absorption observed in the spectrum blueward of Lyα. Eilers et al. (2017) originally noted that J0100+2802 has an unusually small proximity zone ($R_p = 7.1$ proper Mpc, or a luminosity-corrected $R_{p,corr} = 3.1$ proper Mpc). Such a small zone size could imply a short quasar lifetime ($t < 10^5$ yr)—compared to values of $t > 10^6$ yr seen at this epoch in other proximity zone measurements (Eilers et al. 2017) and from jet lifetimes (Connor et al. 2021)—or that the intrinsic quasar luminosity is less than what is observed.

In the case of J0100+2802, Davies et al. (2020) simulated the evolution of 200 massive halos, each with a grid of assumed intrinsic quasar luminosities. The resultant simulated spectra that most closely matched the observed spectrum of J0100+2802 came from quasars with a short lifetime ($\lesssim 10^5$ yr) and the observed luminosity of the quasar, implying that it is not magnified by lensing. Davies et al. (2020) also demonstrated the feasibility of this technique by recovering the known magnification of UHS J0439+1634 (Fan et al. 2019).

To provide an observational counterpart to the simulation-based results of Davies et al. (2020), we turn to the X-ray properties of J0100+2802. Rest-frame X-ray, UV, and IR emission are generated through different processes and from different regions in an AGN. These regions will behave differently as AGN luminosity increases—particularly the X-ray producing corona, which saturates at high luminosities. As such, the flux ratios in these bands provide a marker of the intrinsic luminosity (e.g., Martocchia et al. 2017), and can therefore be used to constrain the magnification of J0100+2802. Here, we reanalyze the X-ray observations of J0100+2802, focusing specifically on how consistent its relative luminosities are with an interpretation that it is magnified by $\mu \sim 450$. Throughout this work we adopt a redshift of $z = 6.327$, based on the [C II] measurements of Wang et al. (2019), and we assume a flat cosmology with $H_0 = 70\,\mathrm{km\,s^{-1}\,Mpc^{-1}}$, $\Omega_M = 0.3$, and $\Omega_\Lambda = 0.7$.

2. X-Ray Observations

J0100+2802 was observed by XMM-Newton for 65 ks in 2016, as previously reported by Ai et al. (2017). We reprocessed these observations using the most current values of the XMM calibrations and of the SAS analysis software, v19.0.0 (Gabriel et al. 2004). To minimize the effects of systematic processing choices, we used the `xmmextractor` routine to generate spectra from the EPIC camera observations, although we manually set the source ($25''$ radius circle) and background regions ($90''-300''$ annulus with sources masked) to avoid contamination.

We note that J0100+2802 was also observed by Chandra in a short (14.8 ks), exploratory observation, as reported by Ai et al. (2016). However, that observation only obtained $\sim 4\%$ of the total net counts obtained by the XMM observations, so we do not include it in our spectral fitting. And, while Chandra has a superior angular resolution to XMM, it is not capable of resolving the small-separation ($0''.2$) images reported by Fujimoto et al. (2020). `BAYMAX`, the current state-of-the-art tool for identifying dual sources in Chandra images, is of limited use for separations below $0''.3$, even if we had $50\times$ the number of Chandra counts to work with (Foord et al. 2019).

The three EPIC spectra were fit simultaneously using the Python implementation of `XSPEC` (Arnaud 1996). We binned our spectra to a minimum of only one count per bin, and so we found our best fits through the minimization of the modified C statistic (Cash 1979; Wachter et al. 1979). X-ray emission was modeled as an absorbed power law, `phabs×powerlaw`, with n_H fixed to $6.21 \times 10^{20}\,\mathrm{cm^{-2}}$ (HI4PI Collaboration et al. 2016). Our best fits with 1σ uncertainties are $\Gamma = 2.23^{+0.16}_{-0.13}$ and normalization $n = 3.55^{+0.32}_{-0.31} \times 10^{-6}$, corresponding to a broadband, unabsorbed, rest-frame luminosity of $L_{2-10} = 4.63^{+0.62}_{-0.51} \times 10^{45}\,\mathrm{erg\,s^{-1}}$ and monochromatic rest-frame luminosity at 2 keV of $L_{2\,keV} = 7.1^{+1.7}_{-1.4} \times 10^{27}\,\mathrm{erg\,s^{-1}\,Hz^{-1}}$. These results are consistent with the previous analyses of the same XMM data by Vito et al. (2019; $L_{2-10} = 4.76^{+0.33}_{-0.31} \times 10^{45}\,\mathrm{erg\,s^{-1}}$) and the (poorly constrained) Chandra results of Ai et al. (2016; $L_{2-10} = 9.0^{+9.1}_{-4.5} \times 10^{45}\,\mathrm{erg\,s^{-1}}$). Ai et al. (2017) find a slightly lower luminosity from their analysis of the XMM data ($L_{2-10} = 3.14^{+0.53}_{-0.48} \times 10^{45}\,\mathrm{erg\,s^{-1}}$).
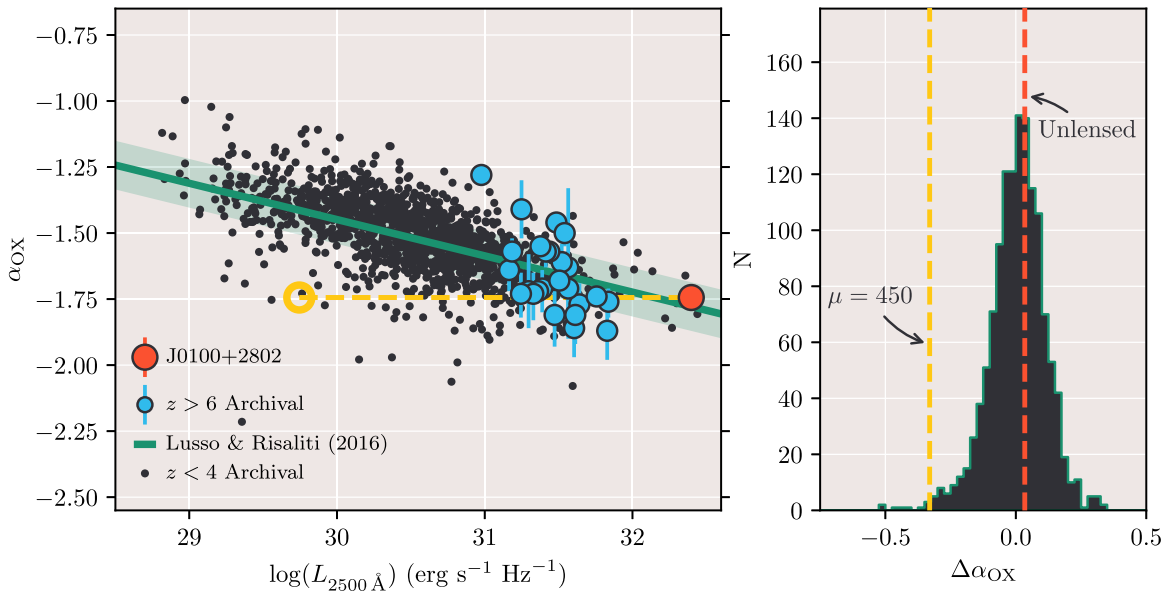
Figure 2. Left: α_{OX} plotted against rest-frame UV monochromatic luminosity at 2500 Å for J0100+2802 (red if unlensed, yellow if magnified by $\mu = 450$), a sample of $z \gtrsim 6$ quasars with archival X-ray and UV data (blue), and low-redshift quasars (black). The predicted best relation from Lusso & Risaliti (2016) and its scatter are shown in green. Right: the distribution of $\Delta\alpha_{OX}$ values for the low-redshift sample. The positions of J0100+2802 assuming no magnification (red) and the Fujimoto et al. (2020) lensed model (yellow) are indicated by the vertical dashed lines. While J0100+2802 is consistent with the predicted relation to within the scatter, it would be X-ray faint if it is magnified by $\mu \sim 450$. Data sources are given in the text.

To enable comparisons to the expectation of the X-ray properties of J0100+2802, we also derive a monochromatic luminosity at rest frame 2500 Å ($L_{2500\,\text{Å}}$) and a rest frame of 6 μm luminosity ($\nu L_{6\,\mu m}$). For the former, we use the fitted spectrum presented by Schindler et al. (2020), adopting $L_{2500\,\text{Å}} = 2.5 \times 10^{32}$ erg s^{-1} Hz^{-1}. For $\nu L_{6\,\mu m}$, we extrapolate from WISE photometry, finding $\nu L_{6\,\mu m} = 1.6 \times 10^{47}$ erg s^{-1}. While there is some uncertainty in this extrapolation, this value is consistent with the modeled mid-IR emission presented by Ai et al. (2017).

3. Comparison to Expectations

One way to assess the expected strength of J0100+2802's X-ray emission is through the optical-to-X-ray flux ratio, α_{OX}.[5] X-ray emission has been observed to flatten as the rest-frame UV luminosity increases, thereby changing α_{OX} with increasing UV luminosity. Magnification from lensing, however, would increase X-ray flux commensurate to the increase in UV brightness, thus leaving α_{OX} unchanged. Here we rely on the best fit of Lusso & Risaliti (2016), who find

$$\log(L_{2\,\text{keV}}) = \gamma \log(L_{2500}) + \beta \pm \sigma, \qquad (1)$$

where $\gamma = 0.642 \pm 0.015$ and $\beta = 6.965^{+0.461}_{-0.465}$ are fit parameters and $\sigma = 0.24$ is the intrinsic scatter. We show this relation (projected into α_{OX}) and the observed values for J0100+2802 in Figure 2; the quasar's X-ray luminosity agrees with the expectation of its UV luminosity, assuming no magnification.

We also show two comparison samples in Figure 2: a sample of $z > 6$ quasars with measured X-ray properties (as compiled by Vito et al. 2021,[6] excluding those values with only upper limits) and the low-redshift sample used by Lusso & Risaliti (2016) to

derive the $L_{2500} - L_{2\,\text{keV}}$ relation. For the latter, we use the scaling relationship derived from the strictest cuts on data quality,[7] but we show quasars filtered by less strict cuts.[8] We note the position where J0100+2802 would intrinsically be were it observed with $\mu = 450$, where it would be X-ray faint. Here, the offset from the predicted relation is $\Delta\alpha_{OX} = -0.33$, corresponding to 3.5σ, based on the intrinsic scatter; by contrast, this is $\Delta\alpha_{OX} = 0.03$ if J0100+2802 is not magnified.

Another test of the expected X-ray luminosity comes from Stern (2015), who characterized a relationship between mid-IR and X-ray luminosities for $z < 4.6$ AGN across almost 6 orders of magnitude, showing that the X-ray emission saturates at the highest mid-IR luminosities. As shown in Figure 3, this saturation produces a distinct curve in the X-ray–mid-IR luminosity plane that, as noted by Stern & Walton (2020), could potentially be used to identify lensed quasars. Lensing will magnify both luminosities equally, so that a lensed galaxy should rise away from the observed, curving relation. For J0100+2802, we have the opposite concern: its observed properties are almost exactly those predicted by the Stern (2015) relation, and, were it lensed by $\mu \sim 450$, it would have to be X-ray faint.

While Stern (2015) do not report the scatter on their fit, we can nevertheless compute how significant a deviation J0100+2802 would be from that relation if lensed. Using the same AGN sample Stern (2015) used to compute the relation (excluding the obscured AGN from the NuSTAR sample), we find a maximum negative offset of $\log(\Delta_X/\text{erg s}^{-1}) = -0.88$. In contrast, the nominal offset from this relation for J0100+2802, assuming $\mu = 450$, is $\log(\Delta_X/\text{erg s}^{-1}) = -1.00$. Furthermore, the Stern (2015) sample has a standard deviation of offsets of $\sigma = 0.376 \log(\text{erg s}^{-1})$, meaning J0100+2802 would be a 2.7σ offset. As such, the lensing scenario proposed by Fujimoto et al. (2020) would not only require J0100+2802 to be one of the most

---

[5] $\alpha_{OX} \equiv 0.3838 \times \log(L_{2\,\text{keV}}/L_{2500})$, where L_ν is the monochromatic luminosity.

[6] These values are originally drawn from Vito et al. (2019), Connor et al. (2019, 2020), Wang et al. (2021b), and Pons et al. (2021).

[7] $E(BV) \leqslant 0.1$, X-ray S/N > 5, and $1.9 \leqslant \Gamma \leqslant 2.8$.

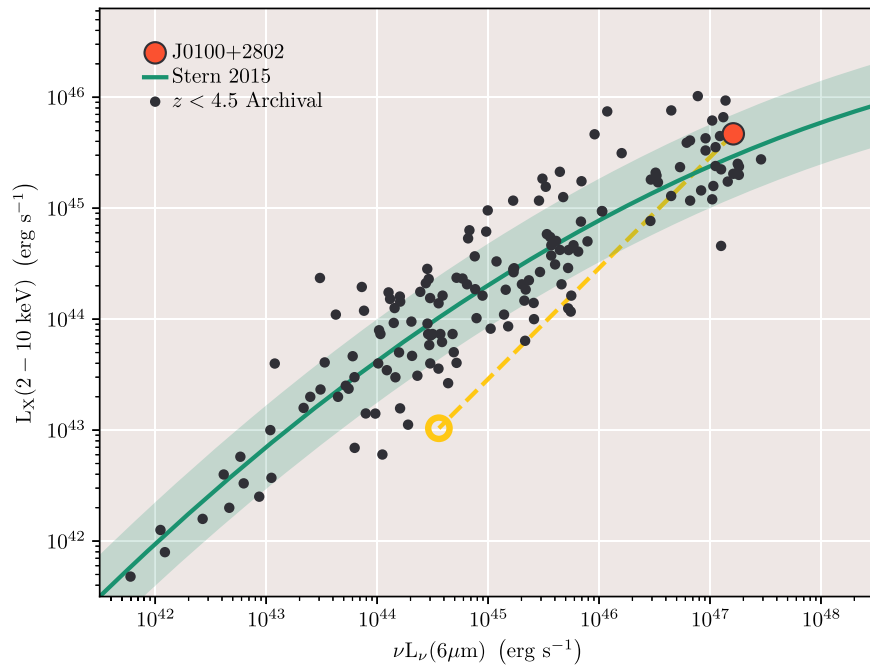[8] $E(BV) \leqslant 0.1$, X-ray S/N > 5, and $\Gamma \geqslant 1.6$.

Figure 3. X-ray luminosity and mid-IR luminosity of J0100+2802 (red) and a sample of lower-redshift unlensed quasars (black, from the compilation of Stern 2015). The scaling relation of Stern (2015) is shown by the green line, with the shaded region corresponding to the standard deviation of offsets in the underlying sample, and the dashed yellow line shows the true position of J0100+2802 if it were being lensed by $\mu \sim 450$. Due to the bend in the X-ray–IR relation caused by the X-ray corona saturating at higher luminosities, lensing causes significant deviations from the nominal relation, as seen here.

extremely lensed quasars known, but it would also have to independently be an extreme outlier in X-ray faintness.

4. Is J0100+2802 X-Ray Faint?

As we have demonstrated above, if J0100+2802 were lensed with a magnification of $\mu \sim 450$, it would be extremely X-ray faint. Indeed, with $\Delta\alpha_{OX} = -0.32$, it would be the second-most X-ray underluminous quasar known at $z > 6$ and potentially even at $z > 4$ (Vito et al. 2021). Here we briefly discuss how likely this scenario is, independent of expectations from scaling relations.

There are three common AGN classifications that are each observed to be X-ray faint: Type 2 (obscured) AGN, broad absorption line (BAL) quasars, and weak emission-line quasars (WLQs, with Lyα+N V equivalent widths of $\lesssim 10$ Å). Type 2 AGN are not intrinsically X-ray weak relative to Type 1 AGN, but their soft X-ray flux is obscured by thick column densities ($n_H \gtrsim 10^{22}$ cm^{-2}; e.g., Rojas et al. 2020), and they can be independently classified from their lack of broad emission lines in their UV/optical spectrum (< 1000 km s^{-1}; e.g., Netzer 2015). In contrast, BAL quasars are intrinsically X-ray weak, even at hard X-ray energies (Luo et al. 2014), and they are characterized by broad absorption lines. We can rule these two classifications out, as deep ESI and X-Shooter spectra show that J0100+2802 is neither type of quasar, with FWHM$_{Mg II} \sim 4000$ km s^{-1} and no broad absorption features (Eilers et al. 2017; Schindler et al. 2020). J0100+2802 is, however, a weak emission-line quasar, with a Lyα+N V equivalent width of ~ 10 Å (Wu et al. 2015).

Numerous studies have found WLQs are more likely to be X-ray faint (e.g., Wu et al. 2012), although the presence of weak lines does not guarantee X-ray weakness. One of the more common diagnostics for WLQs (e.g., Ni et al. 2018) is the strength and velocity of the C IV line ($\lambda 1549.06$ Å), but

Schindler et al. (2020) were unable to model this line in their analysis of J0100+2802 due to significant telluric contamination. However, there are other tracers for X-ray weakness in WLQs, notably the X-ray power-law slope; for J0100+2802, $\Gamma = 2.23^{+0.16}_{-0.13}$, which is a relatively soft value for high-redshift quasars (e.g., Vito et al. 2019). Luo et al. (2015) find that X-ray weak WLQs have much harder X-ray spectra, with $\langle\Gamma\rangle = 1.16^{+0.37}_{-0.32}$, while normal-luminosity WLQs have $\langle\Gamma\rangle = 2.18 \pm 0.09$. Similarly, for a sample of 14 stacked $z \sim 2$ X-ray faint WLQs, Ni et al. (2018) found $\Gamma = 1.19^{+0.56}_{-0.45}$. Furthermore, that work found rest-frame UV color was a predictor of X-ray weakness, being more common in redder quasars. J0100+2802, however, has $\alpha_\lambda = -1.55$ (where $f_\lambda \propto \lambda^{\alpha_\lambda}$), meaning its continuum is a typical color (e.g., Vanden Berk et al. 2001). Thus, J0100+2802 does not have optical properties that would lead to the expectation that it is X-ray faint.

We also directly compare the properties of J0100+2802 to those of other quasars that are significant outliers in $\Delta\alpha_{OX}$. In Figure 2 we show the distribution of $\Delta\alpha_{OX}$ for the sample of Lusso & Risaliti (2016), which has already been trimmed of BAL quasars; additionally, and as noted above, we also excluded sources with Galactic extinctions of $E(B - V) > 0.1$ (following Lusso & Risaliti 2016), those with X-ray signal-to-noise ratios below 5, and those sources with X-ray spectral photon indices of $\Gamma < 1.6$, where the latter is indicative of obscuration (e.g., Ricci et al. 2017). Although the unlensed value of J0100+2802 is consistent with the expectations of Lusso & Risaliti (2016), for the $\mu = 450$ scenario, J0100+2802 resides on the extreme tail of the $\Delta\alpha_{OX}$ distribution. Similarly, if lensed, J0100+2802 would be fainter than the mid-IR prediction at a level unmatched in the Stern (2015) sample.

The Fujimoto et al. (2020) lensing hypothesis requires J0100+2802 to be at the extremes of quasar magnification (cf, e.g., Glikman et al. 2018), while the analysis here shows that it would also have to be a significant outlier in X-ray faintness,
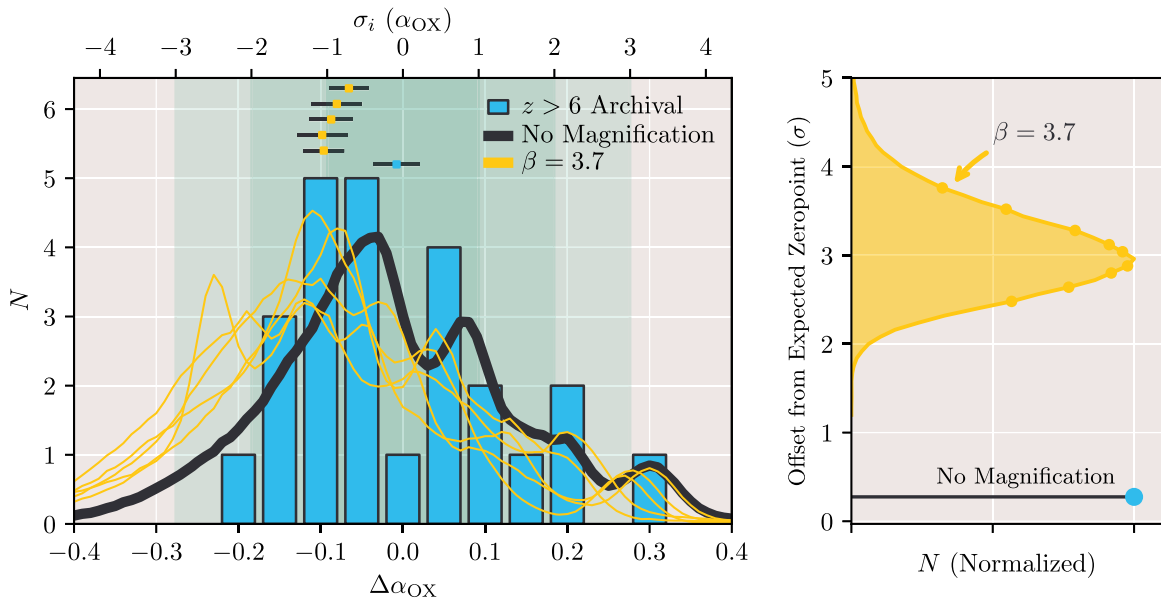
Figure 4. $\Delta\alpha_{OX}$ relative to the Lusso & Risaliti (2016) relation for the additional 25 $z > 6$ quasars with measured X-ray properties (blue). When smoothed by a kernel of width equal to each quasar's individual uncertainties, the distribution is consistent with 0 (black). When the underlying magnification of each quasar is simulated 100,000 times following the Pacucci & Loeb (2020) $\beta = 3.7$ model, this distribution shifts to negative values, with over half of the simulated quasars being fainter than expected by more than the Lusso & Risaliti (2016) intrinsic scatter. Five instances of this simulation are shown in yellow. The average value of $\Delta\alpha_{OX}$ and corresponding standard error on the mean are shown above these distributions when assuming no magnification (blue with black errors) and for the five shown simulations (yellow with black errors). In the right panel, we show the results of the full suite of simulations. Quantified by the mean of $\Delta\alpha_{OX}$ divided by the standard error in the mean, over 50% of simulations have a 3σ or larger tension with the expectations of Lusso & Risaliti (2016). Decile values are indicated by yellow markers.

despite displaying neither the optical nor X-ray characteristics expected for such an object. While, in the infiniteness of the universe, it is possible for a quasar with a 3σ underluminosity to also be lensed by a similarly extreme magnification, these two probabilities are independent, and so Occam's razor leads us to the much simpler conclusion: J0100+2802 is only marginally magnified, at most.

5. Constraints from the Broader Population

Even if we accept enough uncertainty to allow for J0100 +2802 to be an order of magnitude fainter than predicted, there is still one further test. If J0100+2802 were magnified by $\mu \sim 450$, Pacucci & Loeb (2020) argue that we would expect a significant fraction of all known $z > 6$ quasars to be lensed as well. Pacucci & Loeb (2020) find that the detection of a source with such an extreme magnification requires β, the bright-end slope of the luminosity function—such that $\Phi(L) \propto L^{-\beta}$—must be $\beta \geqslant 3.7$. From this value we can derive $P(\mu)$, the probability of an individual quasar being lensed to a certain magnification (Pacucci & Loeb 2019). As such, there is another observable test of the Fujimoto et al. (2020) hypothesis: are the remaining $z > 6$ quasars consistent with being magnified at the level predicted for $\beta = 3.7$?

To test this proposition, we consider the $\Delta\alpha_{OX}$ of all the $z > 6$ quasars plotted in Figure 2. To standardize the analysis, we compute L_{2500} for these objects directly from their measured M_{1450} values, assuming $L_\nu \propto \nu^{-\alpha_\nu}$ and $\alpha_\nu = 0.3$ (e.g., Selsing et al. 2016), and we compare α_{OX} values to those predicted by Lusso & Risaliti (2016). The individual values of $\Delta\alpha_{OX}$ are shown by the blue histogram in Figure 4. To account for uncertainties, we smooth this distribution with a Gaussian kernel sized to each quasar's α_{OX} uncertainty, which is shown by the solid black line. The mean and standard error on the mean for this distribution are -0.008 and ± 0.028, respectively.

For the $\beta = 3.7$ case, we simulate what the values of $\Delta\alpha_{OX}$ would be if each quasar was unmagnified for a randomly drawn value of $P(\mu)$. Magnification probabilities are derived from Pacucci & Loeb (2020), who report $P_{51}(\mu) = \prod_{i=1}^{51}(1 - P_i(\geqslant\mu))$, the cumulative probability that at least one quasar in a sample of 51 is magnified by μ. Here, we assume all quasars have the same inherent lensing probabilities. As this distribution stops at $\mu = 10$, we linearly extrapolate in $\log(P(\geqslant\mu)) - \log(\mu)$ space, in keeping with the distributions shown for $\beta = 3.6$ and $\beta = 2.6$ by Pacucci & Loeb (2019). To reduce the effects of this extrapolation on our results, we conservatively decrease the projected slope by 10%.

We then simulated new distributions of $\Delta\alpha_{OX}$ by probabilistically assigning each quasar an assumed magnification and then computing that quasar's lensing-corrected offset. In more than 50% of our simulations, the average value of $\Delta\alpha_{OX}$ exceeded a 3σ negative offset from 0, quantified by the standard error on the mean; the full distribution of simulation results is shown in the right panel of Figure 4. We also show five individual realizations of the simulation in the left panel, again smoothed by measurement uncertainties.

The implication of these results is that, if J0100+2802 is lensed by $\mu \sim 450$, $z > 6$ quasars must behave fundamentally differently at X-ray energies than at lower redshifts. However, Lusso et al. (2020) have shown that quasars show no evolution in their X-ray to UV relation up to at least $z \sim 5$, while Nanni et al. (2017) report that there is no evolution in the basic X-ray spectral properties up to $z \sim 6$. Furthermore, De Rosa et al. (2014) find no evolution in the emission-line properties (flux ratios and equivalent widths) of $z > 6$ quasars compared to their low-redshift counterparts, while Timlin et al. (2020) find that these emission lines (Mg II and C IV) are tracers of the underlying $L_{2500} - L_{2\,keV}$ relation. And, while there is some evidence that WLQs are more common at higher redshifts (Bañados et al. 2016), the X-ray properties of our sample are

consistent with not being X-ray faint (Vito et al. 2019). As such, the large deviation from the α_{OX} relation required for J0100+2802 to be strongly lensed is in tension with our current understanding of early AGN.

6. Summary

In this Letter, we have examined the claims by Fujimoto et al. (2020) that J0100+2802 is lensed with a magnification of $\mu \sim 450$ through the perspective of the quasar's X-ray properties. In particular, we focus on how the source's X-ray luminosity relates to its rest-frame UV and IR luminosities. We find that, for J0100+2802 to be magnified at this level, it would have to be an extremely yet uncharacteristically intrinsically faint X-ray source. In addition, the implication posed by Pacucci & Loeb (2020) that many $z \gtrsim 6$ quasars are lensed is incompatible with broader trends in AGN evolution established in the wider literature. The quantification of our analysis includes:

1. If lensed by $\mu \sim 450$, J0100+2802 is offset from the Lusso & Risaliti (2016) $L_{2500} - \alpha_{OX}$ relation by $\Delta\alpha_{OX} = -0.32$, which corresponds to 3.5σ, based on the intrinsic scatter. The spectral characteristics of J0100+2802 are not consistent with those of typical quasars that are X-ray faint.
2. If lensed by $\mu \sim 450$, J0100+2802 is offset from the Stern (2015) $L_X - \nu L_{6\,\mu m}$ relation by $\log(L_{2-10\,\mathrm{keV}}) = -1.00$ (2.7σ), which would be larger than any other quasar in the Stern (2015) sample ($N = 155$).
3. If the population of $z > 6$ quasars is lensed following the predictions of Pacucci & Loeb (2020), which are needed to produce a magnification of $\mu = 450$, then these quasars would be in tension with the Lusso & Risaliti (2016) $L_{2500} - \alpha_{OX}$ relation for lower-redshift quasars at a $\gtrsim 3\sigma$ level, despite extensive evidence that the central engines of high-redshift quasars are not significantly different from those of low-redshift quasars.

Further insight into the nature of J0100+2802 should come with the launch of the JWST, as this quasar is the target of guaranteed-time observations, including a spatial investigation of the host galaxy with NIRSpec-IFU (Ferruit et al. 2017). While awaiting those data, we demonstrate here that X-ray observations remain a powerful tool for studying the early universe.

Software: PyFITS (Barrett & Bridgman 1999), SAS (Gabriel et al. 2004), XSPEC (Arnaud 1996).

ORCID iDs

Thomas Connor ⓘ https://orcid.org/0000-0002-7898-7664
Daniel Stern ⓘ https://orcid.org/0000-0003-2686-9241
Eduardo Bañados ⓘ https://orcid.org/0000-0002-2931-7824
Chiara Mazzucchelli ⓘ https://orcid.org/0000-0002-5941-5214

References

Ai, Y., Dou, L., Fan, X., et al. 2016, ApJL, 823, L37
Ai, Y., Fabian, A. C., Fan, X., et al. 2017, MNRAS, 470, 1587
Arnaud, K. A. 1996, in ASP Conference Series 101, Astronomical Data Analysis Software and Systems, ed. G. H. Jacoby & B. Barnes (San Francisco, CA: Freeman), 17
Bañados, E., Venemans, B. P., Decarli, R., et al. 2016, ApJS, 227, 11
Barrett, P. E., & Bridgman, W. T. 1999, in ASP Conference Series 172, Astronomical Data Analysis Software and Systems VIII, ed. D. M. Mehringer, R. L. Plante, & D. A. Roberts (San Francisco, CA: Freeman), 483
Cash, W. 1979, ApJ, 228, 939
Connor, T., Bañados, E., Mazzucchelli, C., et al. 2020, ApJ, 900, 189
Connor, T., Bañados, E., Stern, D., et al. 2019, ApJ, 887, 171
Connor, T., Bañados, E., Stern, D., et al. 2021, ApJ, 911, 120
Davies, F. B., Wang, F., Eilers, A.-C., & Hennawi, J. F. 2020, ApJL, 904, L32
De Rosa, G., Venemans, B. P., Decarli, R., et al. 2014, ApJ, 790, 145
Eilers, A.-C., Davies, F. B., Hennawi, J. F., et al. 2017, ApJ, 840, 24
Fan, X., Wang, F., Yang, J., et al. 2019, ApJL, 870, L11
Ferruit, P., Arribas, S., & Maiolino, R. 2017, NIRSpec-IFU Observations of a QSOs at z = 6, JWST Proposal, Cycle 1
Foord, A., Gültekin, K., Reynolds, M. T., et al. 2019, ApJ, 877, 17
Fujimoto, S., Oguri, M., Nagao, T., Izumi, T., & Ouchi, M. 2020, ApJ, 891, 64
Gabriel, C., Denby, M., Fyfe, D. J., et al. 2004, in ASP Conference Proceedings 314, ADASS XIII, ed. F. Ochsenbein, M. G. Allen, & D. Egret (San Francisco, CA: Freeman), 759
Glikman, E., Rusu, C. E., Djorgovski, S. G., et al. 2018, arXiv:1807.05434
HI4PI Collaboration, Ben Bekhti, N., Flöer, L., et al. 2016, A&A, 594, A116
Luo, B., Brandt, W. N., Alexander, D. M., et al. 2014, ApJ, 794, 70
Luo, B., Brandt, W. N., Hall, P. B., et al. 2015, ApJ, 805, 122
Lusso, E., & Risaliti, G. 2016, ApJ, 819, 154
Lusso, E., Risaliti, G., Nardini, E., et al. 2020, A&A, 642, A150
Martocchia, S., Piconcelli, E., Zappacosta, L., et al. 2017, A&A, 608, A51
Nanni, R., Vignali, C., Gilli, R., Moretti, A., & Brandt, W. N. 2017, A&A, 603, A128
Netzer, H. 2015, ARA&A, 53, 365
Ni, Q., Brandt, W. N., Luo, B., et al. 2018, MNRAS, 480, 5184
Pacucci, F., & Loeb, A. 2019, ApJL, 870, L12
Pacucci, F., & Loeb, A. 2020, ApJ, 889, 52
Pons, E., McMahon, R. G., Banerji, M., & Reed, S. L. 2021, MNRAS, 501, 6208
Ricci, C., Trakhtenbrot, B., Koss, M. J., et al. 2017, ApJS, 233, 17
Rojas, A. F., Sani, E., Gavignaud, I., et al. 2020, MNRAS, 491, 5867
Schindler, J.-T., Farina, E. P., Bañados, E., et al. 2020, ApJ, 905, 51
Selsing, J., Fynbo, J. P. U., Christensen, L., & Krogager, J. K. 2016, A&A, 585, A87
Stern, D. 2015, ApJ, 807, 129
Stern, D., & Walton, D. J. 2020, ApJL, 895, L38
Timlin, J. D., Brandt, W. N., Ni, Q., et al. 2020, MNRAS, 492, 719
Vanden Berk, D. E., Richards, G. T., Bauer, A., et al. 2001, AJ, 122, 549
Vito, F., Brandt, W. N., Bauer, F. E., et al. 2019, A&A, 630, A118
Vito, F., Brandt, W. N., Ricci, F., et al. 2021, A&A, 649, A133
Wachter, K., Leach, R., & Kellogg, E. 1979, ApJ, 230, 274
Wang, F., Fan, X., Yang, J., et al. 2021b, ApJ, 908, 53
Wang, F., Wang, R., Fan, X., et al. 2019, ApJ, 880, 2
Wang, F., Yang, J., Fan, X., et al. 2021a, ApJL, 907, L1
Willott, C. J., Bergeron, J., & Omont, A. 2015, ApJ, 801, 123
Wu, J., Brandt, W. N., Anderson, S. F., et al. 2012, ApJ, 747, 10
Wu, X.-B., Wang, F., Fan, X., et al. 2015, Natur, 518, 512